RSC Advances

ROYAL SOCIETY OF CHEMISTRY

www.rsc.org/advances

Journal Name

ARTICLE

Graphene/$SrTiO_3$ Nanocomposites Used as an Effective Electron-Transporting Layer for High-performance Perovskite Solar Cells

Received 00th January 20xx,
Accepted 00th January 20xx

DOI: 10.1039/x0xx00000x

www.rsc.org/

Chen Wang,[a] Ying Tang,[a] Yajing Hu,[a] Lu Huang,[a] Jianxun Fu,[b] Jing Jin,[a] Weimin Shi,[a] Linjun Wang [a] and Weiguang Yang[a*]

The organic–inorganic perovskite solar cells based on binary oxides have been studying for a long time and obtained impressive advance in performance. However, the study using ternary oxides as electron-transporting layer is scarce and there are still many problems to be solved. The ternary oxide $SrTiO_3$ with a perovskite structure well matched with the perovskite absorber layer in crystal structure. Although the device based on mesoporous-$SrTiO_3$ (mp-$SrTiO_3$) showed a high Voc, its average Jsc is still too low compared with mp-TiO_2 based device. In this work, we used graphene/$SrTiO_3$ nanocomposites as an effective electron-transporting layer, due to the superconductivity of the graphene combined with tuning the amount of the starting graphene to increase the light harvest of absorber layer and decrease recombination centers, we got a great achievement, the advice based on graphene/$SrTiO_3$ nanocomposites exhibited a PCE of 10% with the Jsc of 18.08mA/cm^2, increased by 46.0 and 45.6% respectively compared with mp-$SrTiO_3$ based device, indicating incorporation of graphene is an effective way to improve the Jsc of mp-$SrTiO_3$ based perovskite solar cell.

1. Introduction

As a promising new energy technology, organic–inorganic perovskite solar cells as the third generation solar cell have been attracting a wide range of attention in recent years due to their traits of direct band gap, large absorption coefficient, ambipolar diffusion and long carrier diffusion length.[1-3] The power conversion efficiency (PCE) of this kind of solar cell was expected to up to 20% ,[4] and the highest PCE of 19.3% has already been achieved.[5] Mesoporous-TiO_2 (mp-TiO_2) as an anode material is the most common device architecture in perovskite solar cell. This mp-TiO_2 as an electron-transporting layer extracts photoexcited electrons generated in the absorber layer.[6] The most used nanostructures in constructing perovskite solar cells were anatase TiO_2 nanoparticles, with the highest power conversion efficiency (PCE) of over 17%. Compared with the anatase TiO_2 nanoparticles-based device, the rutile TiO_2 nanoparticles-based device possesses the properties of higher electron diffusion coefficient and lower electron recombination demonstrating a PCE close to 15%.[7] In addition, the nanosheets,[8-10] nanorods, [11-15] nanotubes,[16] nanowires[17-20] and mesoporous single crystals,[21] were also used in the devices based on mp-TiO_2, and no matter what shape they were, their device performances were dramatically affected by the thickness of the mp-TiO_2 layer. The perovskite solar cell showed a higher PCE when it had a thinner mp-TiO_2 layer. Mp-ZnO is a most suitable candidate to replace the mp-TiO_2 attributing to its characteristics of comparable energy levels as well as relatively higher electron mobility.[22,23] Hagfeldt and coworkers reported the Device based on mp-ZnO for the first time.[24] They used ZnO nanorod arrays to fabricate a ITO/bl-ZnO/NRA-ZnO/$MAPbI_3$/spiro-OMeTAD/Ag device, which achieved a PCE of 5%. Park and coworks adjusted the diameter and length of ZnO nanorod arrays improving the PCE to 11.13%.[25] The most efficient device based on ZnO was made by Dianyi Liu and coworkers, the ZnO nanoparticles were assembled with $CH_3NH_3PbI_3$, showing a PCE of 15.7%.[26] Mp-Al_2O_3 as an insulating materials worked only as a scaffold in the perovskite solar cell, the device based on mp-Al_2O_3 was called “meso-superstructured solar cell”, which was first put forward by Snaith and coworkers.[27] In this kind of device the photoexcited electrons were directly transported throughout the perovskite layer instead of injecting into Al_2O_3,which is totally different from TiO_2.[28] Device using mp-Al_2O_3 showed a higher Voc than the TiO_2-based device. Device used the FTO/bl-TiO_2/mp-Al_2O_3/$MAPbBr_3$/PDI/Au structure achieved a Voc as high as 1.3 V.[29] Similar to mp-Al_2O_3 , Mp-ZrO_2 [30,31] and SiO_2[32] are also ideal material for scaffold material and the device performance based on both of them showed a PCE over 10%.

Compared to binary oxides discussed above, the ternary oxides such as $SrTiO_3$, were rarely reported as to perovskite solar cell. $SrTiO_3$ possesses the perovskite structure, provided with lots of physical properties, including superconductivity,[33] ferroelectricity,[34] and thermoelectricity.[35] Electron mobility of bulk SrTiO3 is 5−8 cm2 V S−1 at room-temperature,[36] which is

[a] Department of Electronic Information Materials, School of Materials Science and Engineering, Shanghai University, Shanghai 200444, China.
[b] Key Laboratory of Modern Metallurgy and Materials Processing, School of Materials Science and Engineering, Shanghai University, Shanghai 200072, China.
Email: wgyang@shu.edu.cn

much higher compared with TiO_2 (0.1–4 cm^2 V S−1).[37] Although the band gap of $SrTiO_3$ is analogy to that of TiO_2, its slightly higher conduction band is more suitable to $CH_3NH_3PbI_3$,and due to its high dielectric constant, the charge recombination at the interface will be reduced to some extent. Ashok Bera and coworkers first reported mp-$SrTiO_3$ based perovskite solar cell, which showed a high Voc close to 1V, and by adjusting the thickness of the mp-$SrTiO_3$, A V_{OC} > 1 V could be reliably achieved, which was at the cost of Jsc.[38] Despite the relatively higher V_{OC}, its average Jsc is still too low compared with mp-TiO_2 based device. There is an urgent need to find effective way to improve the Jsc of mesoporous-$SrTiO_3$ (mp-$SrTiO_3$) based perovskite solar cell.

Recently, graphene equipped with unique properties such as excellent optical, thermal and electrical activities,[39-42] has attracted lots of interest. Graphene-TiO_2 composites have been successfully used as the anode material in both dye-sensitized solar cells and perovskite solar cells,[43,44] due to its high transparency and electron mobility, the performance of solar cells based on graphene-TiO_2 composites has been dramatically improved.

In this work, we reported the first use of graphene/$SrTiO_3$ nanocomposites as the effective electron-transporting layer. Owing to its remarkably high charge mobility and electronic conductivity, graphene greatly improved the Jsc of mp-$SrTiO_3$ based perovskite solar cell. The best performance of the solar cell based on graphene/$SrTiO_3$ nanocomposites we obtained exhibited the PCE of 10%, and the short-circuit current density was boosted from 12.42 to 18.08 mA/cm^2 after the adjustment of the graphene content. We attributed the improvement in device performance to the fast electron transfer as well as the decrease of the recombination centers and the increase of the light harvest of the absorber layer, indicating the incorporation of the graphene is an effective way to enhance the Jsc of mp-$SrTiO_3$ based perovskite solar cell.

2. Experimental

2.1 Materials

Titanium(IV)-n-butoxide ($Ti(Bu)_4$) (99+%), tetra-n-butylammonium hydroxide (TBAH) (40 wt% in aqueous solution), strontium hydroxide octahydrate ($Sr(OH)_2.8H_2O$) (99%), diethylene glycoll (DEG) (99%), graphene were purchased from Alfa Aesar.

2.2 Preparation of grapheme/$SrTiO_3$ samples

The grapheme/$SrTiO_3$ samples were synthesized by a solvothermal method. 20ml DEG and 0.13M $Sr(OH)_2.8H_2O$ were added to 50ml beaker ,which was heated to 50 °C and stirred for a 2 h in the oil bath until all the $Sr(OH)_2.8H_2O$ was dissolved, then 5mg graphene was added to the obtained solution ,it was put in the ultrasonic bath for approximately 2h to disperse the graphene, This was followed by adding 0.18M $Ti(Bu)_4$, and stirring for 20 min with a magnetic stirrer, next 4ml TBAH was added to the solution, it was also stirred for 20 min ,the final solution was transferred to Teflon cups in an autoclave held at 200°C for 50 h. A series of nanocomposites of $SrTiO_3$ with a varying amount of graphene were denoted as S, C5, C15, C25, C35, C45, according to the weight of graphene designated as 0mg, 5mg, 15mg, 25mg, 35mg, 45mg, respectively. All the samples were prepared in a similar manner. After cooling naturally to room temperature, the nanocomposites were collected by centrifugation and washed thoroughly with alcohol three times. Finally, Ethylcellulose, lauric acid, and terpineol were added into the resulting products and milled for 2 h to obtain viscous pastes. The nominal composition of sample/terpineol/ethylcellulose/lauric acid was 1/6/0.3/0.1.

2.3 Synthesis of CH_3NH_3I

CH_3NH_3I was prepared according to the reported procedure.[45] CH_3NH_3I was synthesized by reacting 34 mL of methylamine (33% in ethanol) and 30mL hydroiodic acid (57 wt% in water) in the ice bath for 2 h with stirring. The precipitate was recovered by putting the solution on a rotary evaporator and carefully removing the solvents at 50°C. The precipitate was washed three times with diethylether and dried at 60°C in a vacuum oven for 24 h.

2.4 Solar cell fabrication

FTO glasses were etched with Zn powder and diluted HCl and washed by ultrasonication with deionized water, and ethanol. Then the cleaned substrates were coated with Titanium diisopropoxide bis(acetylacetonate) (75% Aldrich) diluted in anhydrous ethanol (1:39, volume ration) by the spin-coating to make a compact layer, next TiO_2 dense layers were sintered at 500 for 20 min. On TiO_2 compact layers, the grapheme/$SrTiO_3$ paste (diluted in anhydrous ethanol) was deposited by spin-coating at 4000 rmp for 30s ,and was annealed at 500℃ for 20 min to produce mp-graphene/$SrTiO_3$ film. The prepared graphene/$SrTiO_3$ films were coated with PbI_2 (99% purity) from a solution 1 mol/L PbI_2 in dimethylformamide with a spin-coating speed of 7000 rpm for 30s, followed by heating to 70℃ for 30min ,after the samples cooling to room temperature, 300 µl of 0.063 M CH_3NH_3I solution in 2-propanol was dropped on the PbI_2-coated substrate loading for 30 s, which was spun at 5,000 rmp for 30s and dried at 100 °C for 15 min. Then the hole transport material (HTM) solution was coated on the FTO/compact TiO_2 /mp-graphene/$SrTiO_3$ /$CH_3NH_3PbI_3$ substrates at 4000 rpm for 30s. The composition of HTM was 0.170 M 2,29,7,79-tetrakis-(N,N-di-p-methoxyphenyl-amine) -9,9-spirobifluorene (spiro-MeOTAD), 0.064 M bis(trifluoromethane)sulfonimide lithium salt (LiTFSI, 99.95%, Aldrich) and 0.198 M 4-tert-butylpyridine (TBP, 96%, Aldrich) in the mixed solvent of chlorobenzene (99.8%, Aldrich) and acetonitrile (99.8%, Aldrich) (chlorobenzene **:** acetonitrile =1 : 0.1 v/v). Samples were left in a desiccator overnight and to finish the devices an 80 nm-thick Ag was deposited on the top of the HTM layer by a thermal evaporation next day. All device fabrication steps were carried out under the atmospheric environment.

3. Results and discussion

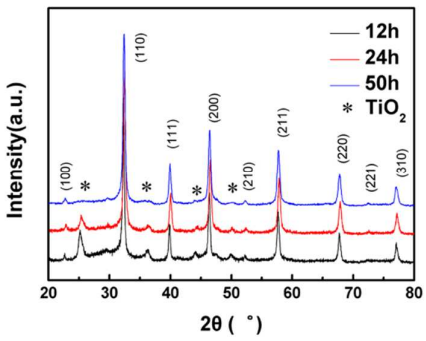

Fig. 1 XRD patterns of graphene/$SrTiO_3$ nanocomposites with different reaction time at 200°C.The * in the Figure represented the peak of TiO_2.

The X-ray powder diffraction (XRD) patterns of as–prepared graphene/$SrTiO_3$ nanocomposites with different solvothermal time at 200°C were given in Fig. 1, which showed the crystalline $SrTiO_3$ has a cubic perovskite structure. The peak centers for $SrTiO_3$ were measured to be 22.66°, 32.30°, 39.86°, 46.38°, 52.22°, 57.68°, 67.70°, 72.54°, 77.08°, corresponding to the (100), (110), (111), (200), (210), (211), (220), (221), (310) crystal planes of $SrTiO_3$ respectively, in agreement with the previous reports.[46,47] The peaks at 25.20°, 36.42°, 44.12°, 49.94° are originated from TiO_2. With the increase of the reaction time, the peak intensity of TiO_2 decreased while that of $SrTiO_3$ increased, indicating that TiO_2 was gradually converted to $SrTiO_3$. When the reaction time was increased to 50h, the peak of byproduct could hardly be seen, showing that the extremely pure $SrTiO_3$ was synthesized. Due to the amount of graphene was too low to detect, the peak of the graphene didn't appear in the XRD patterns.

Fig. 2 showed Scanning electron microscopy (SEM) image of the as-prepared graphene/$SrTiO_3$ product diluted in ethanol and dropped on Si substrate. The $SrTiO_3$ nanoparticles adhered to the graphene flakes tightly, indicating the strong binding force between graphene flakes and $SrTiO_3$ nanoparticles , which is greatly helpful to use graphene flakes as a highway for electron transportation and collection. Since the sample was made without any future process, the cluster of the sample was kind of serious. In spite of the cluster, the outline of both graphene flake and $SrTiO_3$ nanoparticle could still be seen clearly.

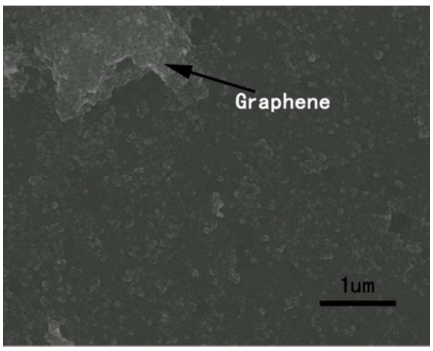

Fig. 2 SEM image of graphene/$SrTiO_3$ nanocomposites on Si substrate.

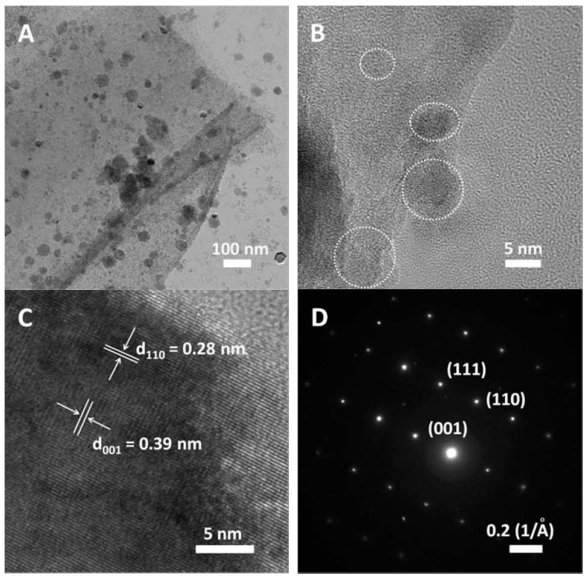

Fig. 3.(A) TEM micrograph of graphene/ $SrTiO_3$ nanocomposites . (B) HRTEM image of graphene/$SrTiO_3$ nanocomposites. (C) HRTEM image of $SrTiO_3$ nanoparticle. (D) SAED pattern of $SrTiO_3$ nanoparticle.

Fig. 3a and b showed Transmission Electron Microscopy (TEM) and high resolution transmission electron microscopy (HRTEM) image of graphene/$SrTiO_3$ nanocomposites. It could be clearly observed that the graphene was monodispersed as nanosheet and $SrTiO_3$ nanoparticles with the diameter varying from 5nm-65nm dispersed in graphene nanosheet. The dotted circle in Fig.3b represented $SrTiO_3$ nanoparticles, adhering to the graphene nanosheet in a random way. The HRTEM image shown in Fig. 3c, showing distinct lattice fringes, The fringe spacing was measured to be 0.39 nm and 0.28 nm, in line with the (001) and (110) planes of the cubic phase of $SrTiO_3$, respectively. The regular crystal diffraction spots in the selected-area electron diffraction (SAED) pattern in Fig.3d matched with cubic perovskite structure $SrTiO_3$, pointing out the good crystallinity of $SrTiO_3$.

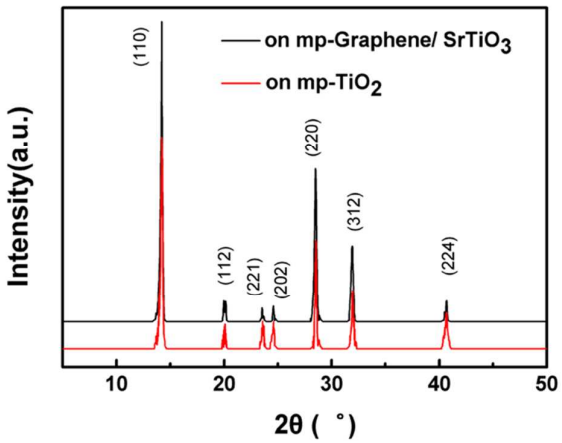

Fig. 4 XRD patterns of the $CH_3NH_3PbI_3$ grown on mp-graphene/$SrTiO_3$ layer and on mp-TiO_2 layer.

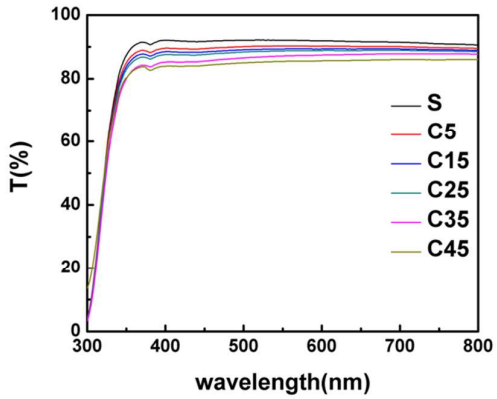

Fig. 5 UV–vis transmission spectrums of mp-graphene/$SrTiO_3$ layer with different graphene content in same thickness.

Fig. 4 showed the XRD patterns for the $CH_3NH_3PbI_3$ grown on mp- graphene/$SrTiO_3$ layer and mp-TiO_2 layer. The peaks at 14.20°, 20.15°, 23.35°, 24.61°, 28.50°, 31.90°, 40.66° could be assigned to the (110), (112), (211), (202), (220), (312), and (224) crystal planes of the tetragonal perovskite structure $CH_3NH_3PbI_3$ respectively, which was in good agreement with the previous work.[48] There was no impurity peaks other than the ones attributable to $CH_3NH_3PbI_3$ to be observed in the XRD patterns, suggesting that $CH_3NH_3PbI_3$ grown on both mp-graphene/$SrTiO_3$ layer and mp-TiO_2 layer was phase pure. While from the patterns it could be seen clearly that the intensity of three strong peaks of the $CH_3NH_3PbI_3$ grown on mp-graphene/$SrTiO_3$ layer was stronger than those on mp-TiO_2 layer, indicting a better crystallization of the $CH_3NH_3PbI_3$ grown on mp-graphene/$SrTiO_3$ layer compared than on mp-TiO_2 layer, which may be attributed to similar crystal structure of the $CH_3NH_3PbI_3$ and $SrTiO_3$ particle and the bigger size of the $SrTiO_3$ particle.

Fig. 5 showed the UV–vis transmission spectrums of mp-graphene/$SrTiO_3$ layers with different graphene content in same thickness. The thinckness of all the samples were 200nm. As shown in Fig. 5, with increasing the graphene content, the transmittance of mp-graphene/$SrTiO_3$ layer decreased obviously. Despite the increase of graphene content, the transmittance is still over 85%, indicating the mp-graphene/$SrTiO_3$ is suitable for being used as anode material.

Fig. 6 showed the UV–vis absorption spectrums of $CH_3NH_3PbI_3$ coated on mp-graphene/$SrTiO_3$ layer and on mp-TiO_2 layer, The thickness of the mp-graphene/$SrTiO_3$ layer and mp-TiO_2 layer was about 200nm.It could be clearly seen the $CH_3NH_3PbI_3$ coated on mp-graphene/$SrTiO_3$ could absorb most light in the visible region. In spite of the difference in graphene content, all the samples showed the similar trend in UV–vis absorption spectra, and the absorbance of different samples were indistinguishable, indicating the strong light absorption of the $CH_3NH_3PbI_3$ on mp-graphene/$SrTiO_3$ layer. Compared to the mp-TiO_2 case, the absorbance of the $CH_3NH_3PbI_3$ on the mp-graphene/$SrTiO_3$ layer was higher when the wavelength was over 500 nm, although its absorbance at shorter wavelength was slightly lower, meaning that the general

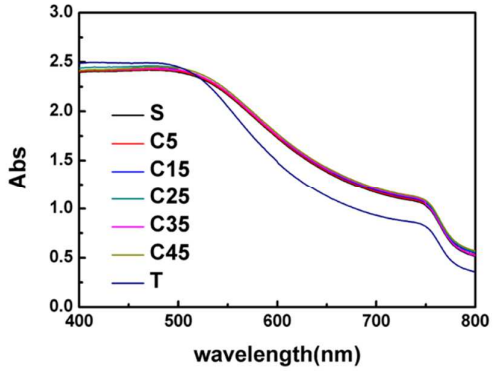

Fig.. 6 UV–vis absorption spectrums of CH3NH3PbI3 on mp-graphene/$SrTiO_3$ layer with different graphene content (S, C5, C15, C25, C35, C45) and on mp-TiO_2 layer (T).

absorption of the $CH_3NH_3PbI_3$ coated on mp-graphene/$SrTiO_3$ layer was higher than that on mp-TiO_2 layer. Compared Fig. 6 with Fig. 5, it could be easily concluded that with the increase of the graphene content, the absorbance of $CH_3NH_3PbI_3$ decreased in fact, since the graphene absorbed part of the light.

The current density–voltage (J–V) curves of the best performing cells of each series were shown in Fig. 7, their corresponding characteristic parameters were given in Table 1. It was obvious that the short-circuit current density and η increased with the increase of the graphene content, and with the further increase of the graphene content, the short-circuit current density and η dramatically decreased. Comparing S with T, it was obvious that the open-circuit voltage of S was higher than that of T, while the short-circuit current density of the S was lower, despite the general absorption of the $CH_3NH_3PbI_3$ coated on mp-$SrTiO_3$ layer was higher than that on mp-TiO_2 layer, which could be attributed to the less efficient carrier collection in the devices based on the mp-$SrTiO_3$ layer. After adding the graphene to the mp-$SrTiO_3$, the short-circuit current density was obviously improved and still maintained the higher open-circuit voltage. The short-circuit current

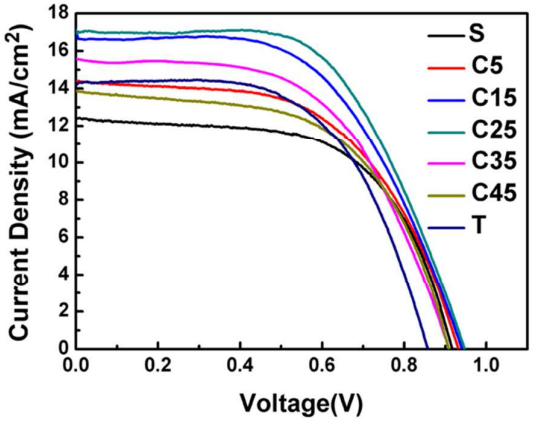

Fig. 7 J–V characteristics of solar cells based on mp-graphene/$SrTiO_3$ nanocomposites with different graphene content (S, C5, C15, C25, C35, C45) and on mp-TiO_2 layer (T) under simulated AM 1.5, 100 mW/cm^2 solar irradiation.

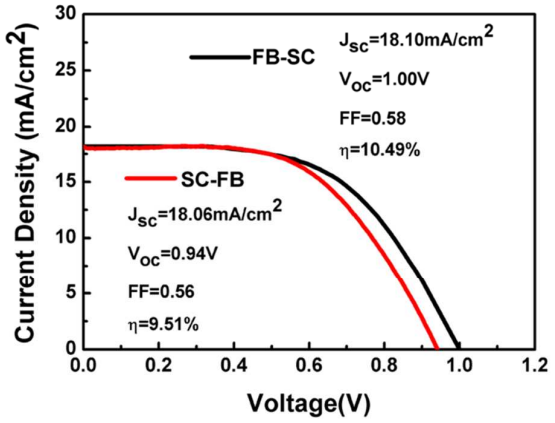

Fig.. 8 The FB-SC and SC-FB J-V curves for the best performing solar cell based on mp-graphene/$SrTiO_3$ nanocomposites under simulated AM 1.5, 100 mW/cm^2 solar irradiation.

Table 1 Parameters for solar cells based on mp-Graphene/ $SrTiO_3$ nanocomposites with different graphene content (S, C5, C15, C25,C35,C45) and on mp-TiO_2 layer (T).

Sample	Jsc(mA/cm^2)	Voc(V)	FF	η(%)
S	12.42	0.92	0.60	6.85
C5	14.38	0.93	0.56	7.49
C15	16.71	0.94	0.56	8.79
C25	17.09	0.95	0.58	9.41
C35	15.60	0.91	0.56	7.94
C45	13.91	0.91	0.56	7.08
T	14.26	0.86	0.59	7.24

density and η of C25 was 17.09 mA/cm^2 and 9.41%, respectively, which increased by 37.6 and 37.3%, relative to S, respectively. Each series based on mp-graphene/$SrTiO_3$ showed an open-circuit voltage over 0.90 V, and almost changed slightly. So the improved performance was obviously attributed to the promoting effect of graphene, which greatly increased the Jsc of the device, due to its fast electron transfer. While with the further increase of the content of graphene, the dramatically decrease in Jsc appeared, which resulted from the decrease in absorbance of $CH_3NH_3PbI_3$ and the increase in recombination of the carriers. As discussed above, with the increase of the density of graphene, the transmittance of the mp-graphene/$SrTiO_3$ layer decreased, which resulted to the decrease in absorbance of $CH_3NH_3PbI_3$, eventually reducing the amount of photo-generated carriers. What's more, the introduce of conductive graphene will introduce new recombination centers and induce the lower photocurrent more or less ,unless the graphene was fully coated with $SrTiO_3$ nanoparticles without direct contact between the graphene and $CH_3NH_3PbI_3$.[49] However, the scale of the graphene flakes we made was very large, much longer than the thickness of the $CH_3NH_3PbI_3$, and taking the aggregation of the graphene which leads to the graphene extending in any direction into account, So with the increase of the density of the graphene, there were unavoidable direct contact between graphene and $CH_3NH_3PbI_3$. By comparing the FF of each series, a slightly decrease could be seen, which could further confirm the presence of the new recombination centers introducing by graphene.

By adjusting the content of graphene to 20 mg, we obtained the best performing solar cell based on graphene/$SrTiO_3$ nanocomposites. Fig. 8 showed the J-V curves for the best performing solar cell with different scanning direction, with the conventional scanning direction from forward bias (FB) to short circuit (SC) we obtained a PCE of 10.49%, while the opposite scanning direction exhibited a PCE of 9.51%. To avoid overestimating the performance of our solar cells, we took the average value of the two different scanning directions. The average values from the J-V curves from different scanning direction exhibited a short-circuit photocurrent of 18.08mA/cm^2, open circuit voltage of 0.97 V, and fill factor of 0.57 producing a PCE of 10%. Compared with S, the short-circuit current density and the PCE were increased by 45.6% and 46.0%, demonstrating the incorporation of graphene did work to increase the Jsc of the $SrTiO_3$-based perovskite solar cell.

4. Conclusions

In conclusion, we succeeded in combining graphene with $SrTiO_3$ as the anode material to fabricate the organic–inorganic perovskite solar cells, Owing to the remarkably high charge mobility and electronic conductivity of graphene, an enhanced short-circuit current density was shown. The content of the graphene greatly affect the performance of the solar cell, excessive graphene decreased the light harvest of absorber layer, and introduced new recombination centers. By changing the amount of graphene to 20mg, we have achieved a remarkable power conversion efficiency of 10% with the short-circuit current density of 18.08 mA/cm^2, open circuit voltage of 0.97 V, which is the best recorded efficiency for $SrTiO_3$-based perovskite solar cell to date. Overall our research made up for the shortcoming of $SrTiO_3$-based perovskite solar cell for its low short-circuit current density compared with conventional TiO_2-based perovskite solar cell, and maintained its relatively high open circuit voltage. However, the FF of our devices was still too low, we will further study to find out the cause.

Acknowledgements

The authors gratefully acknowledge the financial support of the project from the National Science Foundation of China (No. 51202139, 51474142), Nature Science Foundation of Shanghai (No. 12ZR1443900), Specialized Research Fund for the Doctoral Program of Higher education (No. 20123108120022), the Program for Professor of Special Appointment (Eastern Scholar) at Shanghai Institutions of Higher Learning (2012) and the Key Projects in the National Science & Technology Pillar Program (2013BAE07B00).

Notes and references

1 C. V. Kumar, G. Sfyri, D. Raptis, E. Stathatos and P. Lianos, RSC Adv., 2015, 5, 3786.
2 J. J. Choi, X. Yang, Z. M. Norman, S. J. L. Billinge and J. S. Owen, Nano Lett., 2014, 14, 127.
3 Y. Zhao, A. M. Nardes and K. Zhu, J. Phys. Chem. Lett., 2014, 5, 490.
4 N. G. Park, J. Phys. Chem. Lett., 2013, 4, 2423.
5 H. Zhou, Q. Chen, G. Li, S. Luo, T. -b. Song, H.-S. Duan, Z. Hong, J. You, Y. Liu and Y. Yang, Science, 2014, 345, 542.
6 Y. Bai, I. Mora-Sero, F. De Angelis, J. Bisquert and P. Wang, Chem. Rev., 2014, 114, 10095.
7 J. -W. Lee, T. -Y. Lee, P. J. Yoo, M. Grätzel, S. Mhaisalkar and N. -G. Park, J. Mater. Chem. A, 2014, 2 , 9251-9259.
8 L. Etgar, P. Gao, Z. Xue, Q. Peng, A. K. Chandiran, B. Liu, M. K. Nazeeruddin and M. Grätzel, J. Am. Chem. Soc., 2012, 134 , 17396 .
9 M. I. Dar, F. J. Ramos, Z. Xue, B. Liu, S. Ahmad, S. A. Shivashankar, M. K. Nazeeruddin and M. Grätzel, Chem. Mater., 2014, 26, 4675.
10 Y. Rong, Z. Ku, A. Mei, T. Liu, M. Xu, S. Ko, X. Li and H. Han, J. Phys. Chem. Lett., 2014, 5, 2160.
11 H. S. Kim, J. W. Lee, N. Yantara, P. P. Boix, S. A. Kulkarni, S. Mhaisalkar, M. Grätzel and N. G. Park, Nano Lett., 2013, 13, 2412.
12 K. Manseki, T. Ikeya, A. Tamura, T. Ban, T. Sugiura and T. Yoshida, RSC Adv., 2014, 4, 9652.
13 J. Qiu, Y. Qiu, K. Yan, M. Zhong, C. Mu, H. Yan and S. Yang, Nanoscale, 2013, 5, 3245.
14 H. Chen, Z. Wei, K. Yan, Y. Yi, J. Wang and S. Yang, Faraday Discuss., 2014,176, 271.
15 M. Yang, R. Guo, K. Kadel, Y. Liu, K. O'Shea, R. Bone, X. Wang, J. He and W. Li, J. Mater. Chem. A, 2014, 2, 19616.
16 X. Gao, J. Li, J. Baker, Y. Hou, D. Guan, J. Chen and C. Yuan, Chem. Commun., 2014, 50, 6368.
17 Y. M. Xiao, G. Y. Han, Y. P. Li, M. Y. Li and J. H. Wu, J. Mater. Chem. A, 2014, 2, 16856.
18 S. Dharani, H. K. Mulmudi, N. Yantara, P. T. Thu Trang, N. G. Park, M. Gräetzel, S. Mhaisalkar, N. Mathews and P. P. Boix, Nanoscale, 2014, 6, 1675.
19 Q. Jiang, X. Sheng, Y. Li, X. Feng and T. Xu, Chem. Commun., 2014, 50, 14720.
20 Y. Yu, J. Li, D. Geng, J. Wang, L. Zhang, T. L. Andrew, M. S. Arnold and X. wang, ACS Nano., 2015, 9, 564.
21 E. J. Crossland, N. Noel, V. Sivaram, T. Leijtens, J. A. Alexander-Webber and H. J. Snaith, Nature, 2013, 495, 215.
22 Q. Zhang, C. S. Dandeneau, X. Zhou and G. Cao, Adv. Mater., 21, 4087.
23 J. A. Anta, E. Guill´en and R. Tena-Zaera, J. Phys. Chem. C, 2012, 116, 11413.
24 D. Bi, G. Boschloo, S. Schwarzmuller, L. Yang, E. M. Johansson and A. Hagfeldt, Nanoscale, 2013, 5, 11686.
25 D. Y. Son, J. H. Im, H. S. Kim and N. G. Park, J. Phys. Chem. C, 2014, 118, 16567.
26 D. Liu and T. L. Kelly, Nature Photonics, 2014, 8, 133-138.
27 M. M. Lee, J. Teuscher, T. Miyasaka, T. N. Murakami and H. J. Snaith, Science, 2012, 338, 643.
28 Y. H. Hu, Adv. Mater., 2014, 26, 2102.
29 E. Edri, S. Kirmayer, D. Cahen and G. Hodes, J. Phys. Chem. Lett., 2013, 4, 897.
30 D. Bi, S.-J. Moon, L. Häggman, G. Boschloo, L. Yang, E. M. J. Johansson, M. K. Nazeeruddin, M. Grätzel and A. Hagfeldt, RSC Adv., 2013, 3, 18762.
31 H. S. Kim, I. Mora-Sero, V. Gonzalez-Pedro, F. Fabregat-Santiago, E. J. Juarez-Perez, N. G. Park and J. Bisquert, Nat. Commun., 2013, 4, 2242.
32 S. H. Hwang, J. Roh, J. Lee, J. Ryu, J. Yun and J. Jang, J. Mater. Chem. A, 2014, 2, 16429.
33 K. Ueno, S. Nakamura, H. Shimotani, A. Ohtomo, N. Kimura, T. Nojima, H. Aoki, Y. Iwasa and M. Kawasaki, Nat. Mater., 2008, 7, 855.
34 M. Dawber, K. M. Rabe and J. F. Scott, Rev. Mod. Phys., 2005, 77, 1083.
35 H. Ohta, S. Kim, Y. Mune, T. Mizoguchi, K. Nomura, S. Ohta, T. Nomura, Y. Nakanishi, Y. Ikuhara, M. Hirano, H. Hosono and K. Koumoto, Nat. Mater., 2007, 6, 129.
36 O. N. Tufte and P. W. Chapman, Phys. Rev., 1967, 155, 796.
37 Q, Zhang, C. S. Dandeneau, X. Zhou and G. Cao, Adv. Mater., 2009, 21, 4087.
38 A. Bera, K. Wu, A. Sheikh, E. Alarousu, O. F. Mohammed and T. Wu , J. Phys. Chem. C , 2014, 118, 28494.
39 J. –H. Chen, C. Jang, S. Xiao, M. Ishigami and M. S. Fuhrer, Nat. Nanotechnol., 2008, 3 , 206.
40 A. K. Geim and K. S. Novoselov, Nat. Mater., 2007, 6 , 183.
41 S. V. Morozov, K. S. Novoselov, M. I. Katsnelson, F. Schedin, D. C. Elias, J. A. Jaszczak and A. K. Geim, Phys. Rev. Lett., 2008, 100 , 016602.
42 H. Mao, F. Hu, Q. –L. Ye, Y. Xu, X. Yang and B.Lu, Nanoscale, 2014, 6, 8149.
43 L. Chen, Y. Zhou, W. Tu, Z. Li, C. Bao, H. Dai, T. Yu, J.Liu and Z. Zou, Nanoscale, 2013, 5, 3481.
44 J. J.Wang, J. M. Ball, E. M. Barea, A. Abate, J. A. Alexander-Webber, J. Huang, M. Saliba, I. Mora-Sero, J. Bisquert, H. J. Snaith and R. J. Nicholas, Nano Lett., 2014, 14, 724.
45 S. R. Jang, K. Zhu, M. J.Ko, K. Kim, C.Kim, N. G. Park, and A. J.Frank, ACS Nano, 2011, 5, 8267.
46 S. Ouyang, H. Tong, N. Umezawa, J. Cao, P. Li, Y. Bi, Y. Zhang and J. Ye, J. Am. Chem.Soc., 2012, 134, 1974.
47 J. Zhang, J. H. Bang, C. Tang and P. V. Kamat, ACS Nano., 2010, 4, 387.
48 N. J. Jeon, J. H. Noh, Y. C. Kim, W. S. Yang, S. Ryu and Sang Il Seok, Nature Materials, 2014,13, 897.
49 J. T. Wang, J. M. Ball, E. M. Barea, A. Abate, J. A. Alexander-Webber, J. Huang, M.Saliba, I. Mora-Sero, J. Bisquert, H. J. Snaith, and R. J. Nicholas, Nano Lett., 2014, 14, 724.